Bulletin of the Seismological Society of America, Vol. 96, No. 5, pp. 1649–1661, October 2006, doi: 10.1785/0120050119

Tsunami Hazards Associated with the Perachora Fault at Eastern Corinth Gulf, Greece

by G-Akis Tselentis, Faidra Gkika, and Efthimios Sokos

Abstract We investigate the tsunami hazard associated with the Perachora fault at eastern Corinth Gulf, Greece. Realistic faulting parameters are used to model expected coseismic displacements of the seafloor. This study also investigates the effect that rupture complexity has on the local tsunami wave field. Several earthquake scenarios are used as initial conditions for tsunami stimulation either considering the numerous published constant slip models or taking into account the fault rupture complexity with the help of a realistic finite-extent k^{-2} stochastic kinematic source model with k-dependent rise time. The obtained results indicate that there is substantially more variation in the local tsunami wave field derived from the inherent complexity of the shallow fault zone than predicted by a simple elastic dislocation model. Rupture complexity, as represented by heterogeneous slip-distribution patterns, has an important effect on near-field tsunami records. Tsunami hazards assessments based on only a few scenario earthquakes may not accurately account for natural variation in tsunami amplitude caused by earthquake rupture complexity.

Introduction

The coastal area of eastern Corinth Gulf is subjected to a near-field hazard—a tsunami generated in something under a few minutes tsunami travel time to the locality. Such a tsunami can propagate in any direction and thus, depending on the location of the source, path of propagation, and nearshore morphology, form a risk to any vulnerable coastline.

To understand and discuss tsunami danger for the eastern Corinth Gulf region, appropriate numerical modeling, and comparison of model results with the existing information are necessary and effective tools.

It seems that the coasts of the Corinth Gulf have been struck frequently by tsunamis. The paucity of direct records, however, makes a rigorous estimation of the expected tsunami amplitudes rather difficult, and the analysis of available documents remains somehow controversial. Based on historical information, many tsunami-like waves have been reported in the Corinth Gulf. Recently, Papadopoulos (2003) prepared a new list of tsunamis in the Corinth Gulf, and on the basis of these data he tried to assess the cumulative frequency of tsunamis for this specific region. The accuracy of such estimates is low because of data deficiency and the need to adopt relationships linking earthquakes to tsunamis that may not be empirically well grounded. This means that in many cases alternative approaches to evaluate tsunami hazard are to be invoked (Tinti and Armigliato, 2003). Most often, a solution to the problem is searched for in terms of a scenario that is considering the largest event known to have hit the area of interest in the past history and to simulate that event through numerical modeling.

The tsunami modeling process can be divided into three parts: generation, propagation, and run-up (Titov and Gonzalez, 1997). The generation phase includes the formation of an initial disturbance on the ocean surface due to a coseismic deformation of the seafloor. In this case, the initial condition for the long wave propagation is obtained directly from the expected coseismic deformation of the earth's surface. The seafloor deformation field modeled by the corresponding elastic dislocation model is translated directly to the water surface and used as an initial condition for the propagation and run-up phases.

Numerical simulation of the tsunamigenic domain of Perachora fault and the effect that rupture complexity has on the local tsunami wave field is the main goal of this article. This region is of particular interest because many earthquakes have generated observed tsunamis in the past. Furthermore, during the past decades, the region of eastern Corinth Gulf serves as one of the main holiday resorts of Athens and the cities of Corinth, Xylocastro, and Loutraki have been rapidly expanding toward the coastal region (Fig. 1). This growth of population densities on the coast raises a significant hazard for future tsunami that would strike the region.

Although large earthquakes frequently generate substantial submarine landslides in the epicentral area that could generate tsunamis, this study focuses only on tectonic deformation mechanisms from submarine faulting. A numerical model based on shallow-water theory is briefly described in a following section. The time histories of water-

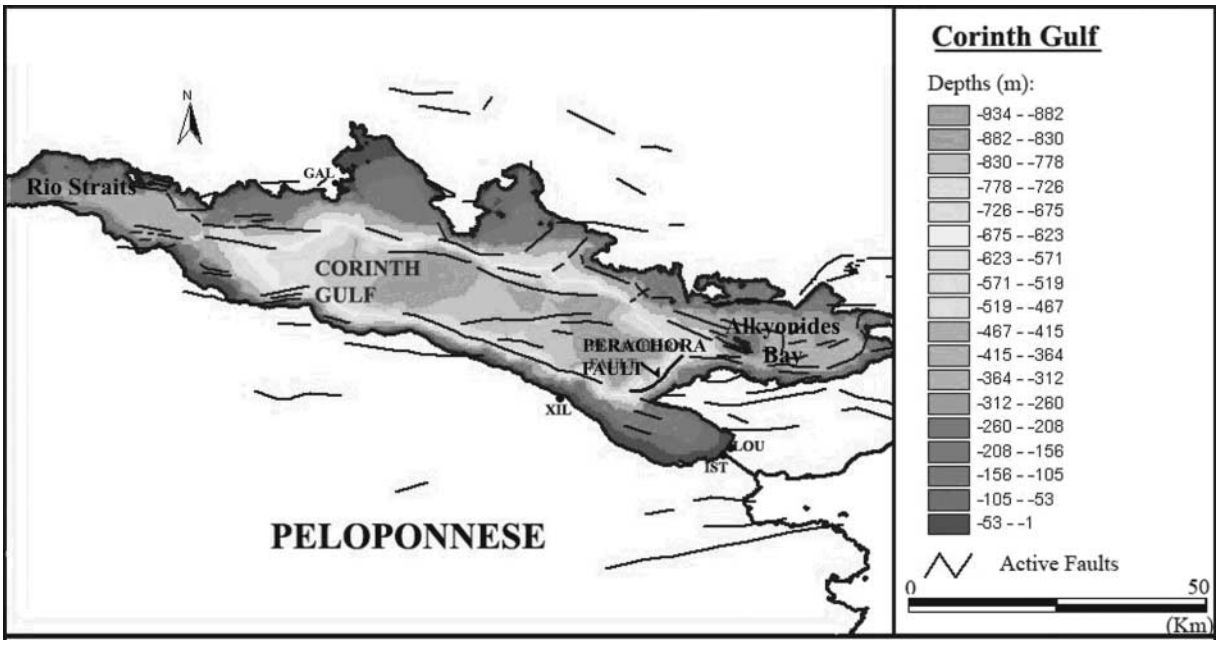

Figure 1. Sea-bottom topography in Corinth Gulf depicting Perachora fault and all known active faults. The coastal cities of Galaxidi (GAL), Xilokastro (XIL), Loutraki (LOU), and Corinth (nearby with Isthmos-IST) are also shown.

surface fluctuations at selected locations are also calculated. A 3D time visualization of the expected tsunami wave field all over the Corinth Gulf is also derived.

Tectonic and Tsunamigenic Environment of Eastern Corinth Gulf

The Gulf of Corinth is an elongated fjord-like basin in central Greece, extending from the Rio straits in the west, to the Alkyonides Bay in the east (Fig. 1). It has a total length of approximately 115 km and a width ranging from approximately 10 to 30 km. The maximum water depth is about 900 m in the center of the Gulf. The present-day Gulf occupies about 2400 km^2 out of a total of approximately 4100 km^2 that correspond to the area extent of the Corinth rift (Stefatos *et al.*, 2002; Moretti *et al.*, 2003).

According to neotectonic studies (e.g., Roberts and Jackson, 1991; Doutsos and Poulimenos, 1992), focal mechanism solution studies (e.g., Tselentis and Makropoulos, 1986; Hatzfeld *et al.*, 2000), and seismic profiling studies (Brooks and Ferentinos, 1984), the extension has an approximately north–south to north-northeast–south-southwest direction. The location of the Corinth Gulf active faults are depicted in Figure 1. However, from a tsunamigenic point of view, only a few of these faults have been linked with tsunamis (Papadopoulos, 2003). In the present investigation we study the tsunami hazard of eastern Corinth Gulf, a region with densely populated holiday resorts.

Along the northwest coast of the Perachora peninsula, striking northeast–southwest, almost parallel to the coastline, lies the offshore Perachora fault (Figs. 1 and 2). The

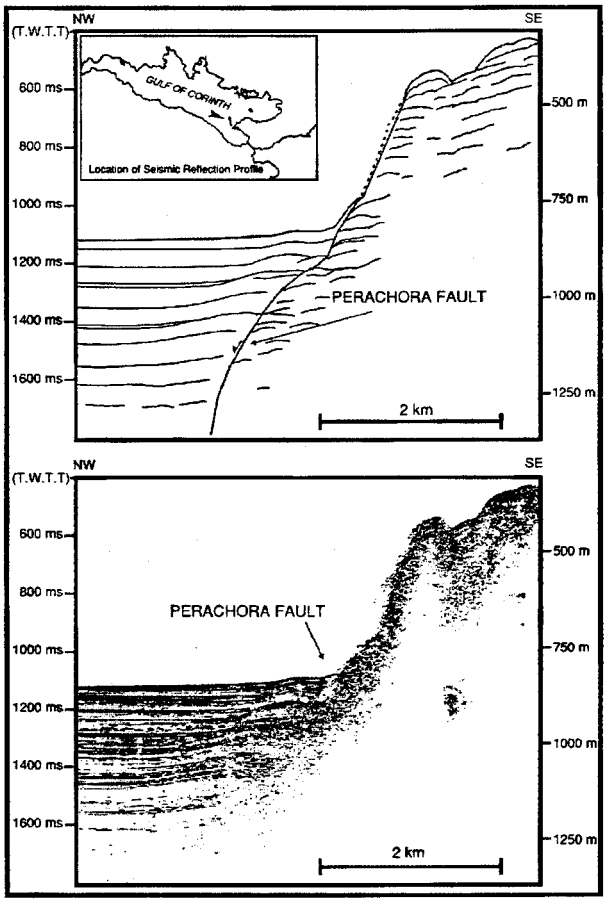

Figure 2. Seismic reflection imaging of the Perachora fault (Brooks and Ferentinos, 1984).

1981 earthquakes provided the opportunity to gather new geological and geophysical data offshore to improve the knowledge of the Perachora fault characteristics, in its emerged part, an issue critical to understanding its tsunamigenic potential. This fault has a length of about 12 km and develops a scarp of 600 m (Stefatos *et al.*, 2002), shifting the Gulf's southern margin fault zone to the north. Seismic profiles (Brooks and Ferentinos, 1984; Sakellariou *et al.*, 1998; Stefatos *et al.*, 2002) indicate a dip between 32° and 48° (Fig. 2).

Elastic Dislocation Modeling

Most studies of earthquake-generated tsunamis use elastic dislocation theory to predict the coseismic seafloor deformation based on fault rupture models (e.g., Satake and Somerville, 1992; Geist, 1999). Many tsunami-hazard assessments are based on a simplified elastic dislocation model constrained by the seismic moment for an earthquake. Rupture complexity is not considered in these cases and the slip is specified as being spatially uniform over the entire rupture area or over several subevents that span the width of the rupture zone. These studies often find that earthquake source models involving spatially uniform slip over a simple rupture surface underestimate the observed tsunami run-up (Legg *et al.*, 2002; Synolakis *et al.*, 1997; Geist, 2002).

Shallow earthquakes occurring offshore produce a seafloor coseismic deformation that can trigger a perturbation of the sea surface. In general, it is accepted that the coseismic deformation is much more rapid than the characteristic time involved in the wave propagation, and that the length scale of this seafloor deformation is much larger than the water depth. These hypotheses allow defining the initial sea-surface deformation as being equal to the coseismic vertical displacement. Analytical formulas established by Okada (1985) to obtain the displacements due to an elastic dislocation allow computing this coseismic deformation, as a function of the fault geometry and the ground elastic parameters. The fault parameters and the seismic moment M_0 are provided by the moment tensor analysis of seismic waves.

Initial conditions for tsunami propagation from Perachora fault are determined from the static displacement field by using the three-dimensional elastic boundary element method (BEM) algorithm POLY-3D (Thomas, 1993) assuming a Poisson's ratio of 0.25.

In general, seismic moment is a good indicator of far-field tsunami amplitude. Near the earthquake source, however, there is a substantial variation of local tsunami amplitude with M_0 (Geist, 2002). A single constant slip scenario fails to account for the highly variable nature of earthquake and tsunami phenomena. The effect of slip variation will be examined in detail in a following section. First, we deal with all published source models concerning Perachora fault 1981, m_b 6.7 earthquake, which are depicted in Table 1.

Taking into consideration the results of the seismic survey in the location of Perachora fault (e.g., Brooks and Ferentinos, 1984), we assume a dip of 45° and fault dimensions 12 km × 12 km and, using these parameters and the seismic moment calculated from each researcher, we derive the corresponding fault slip (Table 2).

Next, we calculate the sea-bottom strain field for each one of the seven fault scenarios. The obtained results are presented in Fig. 3, and the corresponding maximum displacements are depicted in Table 2. Judging from these results we see that there is considerable variation in the resulting sea-bottom deformation.

As mentioned by Legg *et al.* (2002), one area of concern is that the elastic dislocation model produces relatively smaller vertical displacements than the maximum fault slip on the modeled fault surfaces. This result may be reasonable for buried fault sources where no surface rupture occurs (e.g., Plafker and Galloway, 1989). However, where surface fault rupture or for submarine earthquakes, seafloor fault rupture, the maximum surface displacements often equal or approach the maximum subsurface-displacement values derived through seismological observations (Treiman *et al.*, 2002).

Because we typically observe only about one-half the maximum subsurface slip value as surface displacement in the elastic dislocation model, we propose that our estimates of seafloor uplift and initial tsunami wave height may be too low by a similar amount (about 50%). This proposition appears to be supported by observations of recent tsunamis around the world where the measured maximum run-up values also tend to be about twice the predicted values from elastic dislocation models of tectonic faulting based on seismological observations (Geist, 2002).

Mathematical Model

Numerical simulations are useful tools for analyzing tsunami propagation and coastal amplification. The tsunami waves generated by earthquakes depend on the size and the impact of the source mechanism on the displaced water. In the present investigation we concentrate on earthquake-triggered tsunamis only.

Despite differences in the underlying physics of wave propagation in the sea and solid earth, the tsunami wave field emanating from an earthquake source can be thought of as an extension to the seismic wave field (Okal, 1982).

There are at least three kinds of tsunami propagation and inundation models in common use among tsunami scientists: nonlinear shallow-water models (NSWMs), Boussinesq-type long-wave models, and complete fluid dynamics models, which all stem from the work of Peregrine (1967). NSWMs possess some distinctive advantages that make them very suitable for modeling flows occurring in shallow depths (Brocchini *et al.*, 2001). We perform our study with the nonlinear shallow-water wave model.

Since tsunami wavelengths are much larger than the sea depth, tsunamis are considered as shallow-water waves following the long-wave theory.

Table 1
Published Fault Parameters of Perachora Fault, m_b 6.7, 1981 Earthquake

Author	Strike (deg)	Dip (deg)	Rake (deg)	Slip (cm)	Length (km)	Width (km)	M_0 (10^{18} N m)	Depth* (km)
Jackson *et al.* (1982)	300	45	−74	115	15	10	7.28	10
Dziewonski and Woodhouse (1983)							12.9	20
Kim and Kulhanek (1984)	285	45	−70	37	28	17	8.1	12
Bezzeghoud *et al.* (1986)					20	12	10	6
Taymaz *et al.* (1991)	264 ± 15	42 ± 5	−80±				8.75	12 ± 2
Ekstrom and England (1989)							9.01	10
Abercombie *et al.* (1995)				70	18	8	6.04 ± 2.4	5

*Depth refers to hypocentral depth.

Table 2
Fault Parameters Used for the Tsunami Simulation

Perachora Offshore Fault	Dip (deg)	Length (km)	Width (km)	Slip (cm)	$d^{*\dagger}$ (km)	Computed Max Bottom Vertical Displacements (cm)
Jackson *et al.* (1982)	45	12	12	153	5.75	46.28
Dziewonski and Woodhouse (1983)	45	12	12	271	15.75	24.05
Kim and Kulhanek (1984)	45	12	12	170	7.75	38.2
Bezzeghoud *et al.* (1986)	45	12	12	210	1.75	124.8
Taymaz *et al.* (1991)	45	12	12	184	7.75	41.35
Ekstrom and England (1989)	45	12	12	189	5.75	57.17
Abercombie (1995)	45	12	12	126	0.75	90.61

$^{\dagger}d^*$ is the depth to the fault plane.

Long-wave theory is used (where the ratio of water depth to wavelength is small), for which the vertical acceleration of water particles is negligible compared with the gravitational acceleration, and the hydrostatic pressure approximation is used. The nonlinear terms are kept for their use where needed, which is the case in very shallow water (from the tsunami point of view). In addition, we are interested in this investigation on near-field tsunamis, that is, those whose propagation distance is less than 200 km. Hence forth, Cartesian coordinates can be used. The vertical integrated governing equations (Dean and Dalrymple, 1984) can be written (after setting the momentum correction factors equal to unity, with Coriolis effect omitted):

$$\frac{\partial M}{\partial t} + \frac{\partial}{\partial x}\left(\frac{M^2}{D}\right) + \frac{\partial}{\partial y}\left(\frac{MN}{D}\right) + gD\frac{\partial \eta}{\partial x} + \frac{gn^2}{D^{7/3}} M\sqrt{M^2 + N^2} = 0 \quad (1)$$

$$\frac{\partial N}{\partial t} + \frac{\partial}{\partial y}\left(\frac{N^2}{D}\right) + \frac{\partial}{\partial x}\left(\frac{MN}{D}\right) + gD\frac{\partial \eta}{\partial y} + \frac{gn^2}{D^{7/3}} N\sqrt{M^2 + N^2} = 0 \quad (2)$$

$$\frac{\partial \eta}{\partial t} + \frac{\partial M}{\partial x} + \frac{\partial N}{\partial y} = 0, \quad (3)$$

where η is the water surface elevation, t is time, x and y are the horizontal coordinates in zonal and meridional directions, and M and N are the discharge fluxes in the horizontal plane along x and y coordinates,

$$M = U(h + \eta) = UD \quad (4)$$

$$N = V(h + \eta) = VD, \quad (5)$$

where U and V are the vertically averaged horizontal particle velocities and $D = h(x, y) + \eta$ is the total water depth, $h(x, y)$ is the undisturbed basin depth, g is the gravity acceleration, and k is the bottom friction coefficient.

These equations are the fundamental equations used in this article.

The way the bottom friction terms (Fujima *et al.*, 2002) are represented in the preceding equations is explained in brief. After the vertical integration the friction terms appear as τ_{bx}/ρ and τ_{by}/ρ in the x and y momentum equations, respectively, where ρ is the water density. The most widely used roughness factor coefficient is the so-called Manning's n, in which case the bottom friction, τ_b, is expressed as

$$\tau_{bx} = \frac{\rho g n^2}{D^{1/3}} U|U^2 + V^2|^{1/2} \quad (6)$$

$$\tau_{by} = \frac{\rho g n^2}{D^{1/3}} V|U^2 + V^2|^{1/2} \quad (7)$$

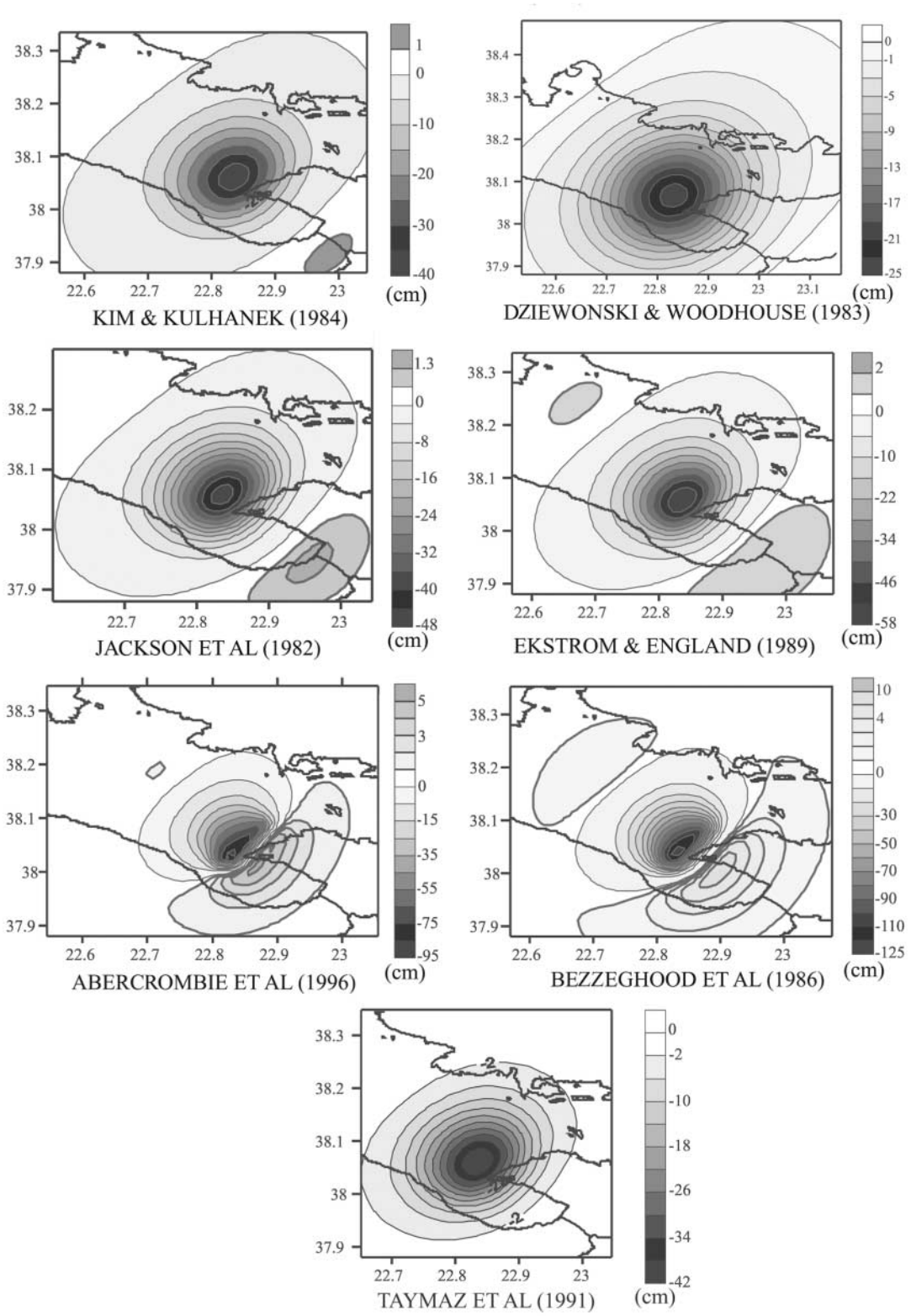

Figure 3. Sea-bottom vertical displacement calculated for each one of the source mechanisms depicted in Table 1. Maximum obtained sea-bottom displacements are listed in Table 2. Positive displacement values are depicted by thicker contours.

After substituting for M and N from equations (4) and (5) we get the friction terms as shown in equations (1), (2), and (3). Although the effect of friction is significant, it is not well understood and a full treatment of the problem would involve the introduction of a bottom-boundary layer (i.e., Svendsen and Putrevu, 1994). Fujima (2001) investigated theoretically and experimentally how bottom obstacles (not negligible but smaller than the numerical grid size) should be considered in tsunami numerical simulations, based on a shallow-water equation. He found that in the most realistic tsunami simulation, roughness coefficient is given by a simple distribution and the value is generally about 0.02 to 0.05 and increases as obstacle height and incident wave height increases. Because the frictional force is inversely proportional to the local water depth D (equations 7 and 8), it has increasingly strong effects as the depth decreases. We thus expect it to affect the flow velocities most where the water is shallowest, that is, inside the swash zone. For the simulation reported here and considering the prevailing bottom morphological features n has been set equal to 0.025.

The model used in this simulation is using the procedure proposed by Goto and Ogawa (1992), using a set of nested grids, where the grid resolution increases in the coastal areas that are to be studied in greater detail.

Another reason for increasing the resolution as we go into shallower water is the fact that (Shuto *et al.*, 1986) each tsunami wavelength should be covered by at least 20 grid points to diminish numerical dispersion (dissipation). Ramming and Kowalik (1980) found that 10 grid points per wavelength is sufficient if we are willing to accept a 2% error in the phase velocity. Another reason is that numerical stability considerations (Courant-Friedrichs-Lewy or CFL stability criterion) require that the finite differences timestep be such that

$$\Delta t \leq \frac{\Delta x}{\sqrt{2gh_{\max}}}, \tag{8}$$

where Δx is the space discretization size, g is the gravitational acceleration, and $h_{\max}$ is the maximum still-water depth in the given grid. This is an ordinary way to select the temporal and spatial grids, if run-up is not included in sim-

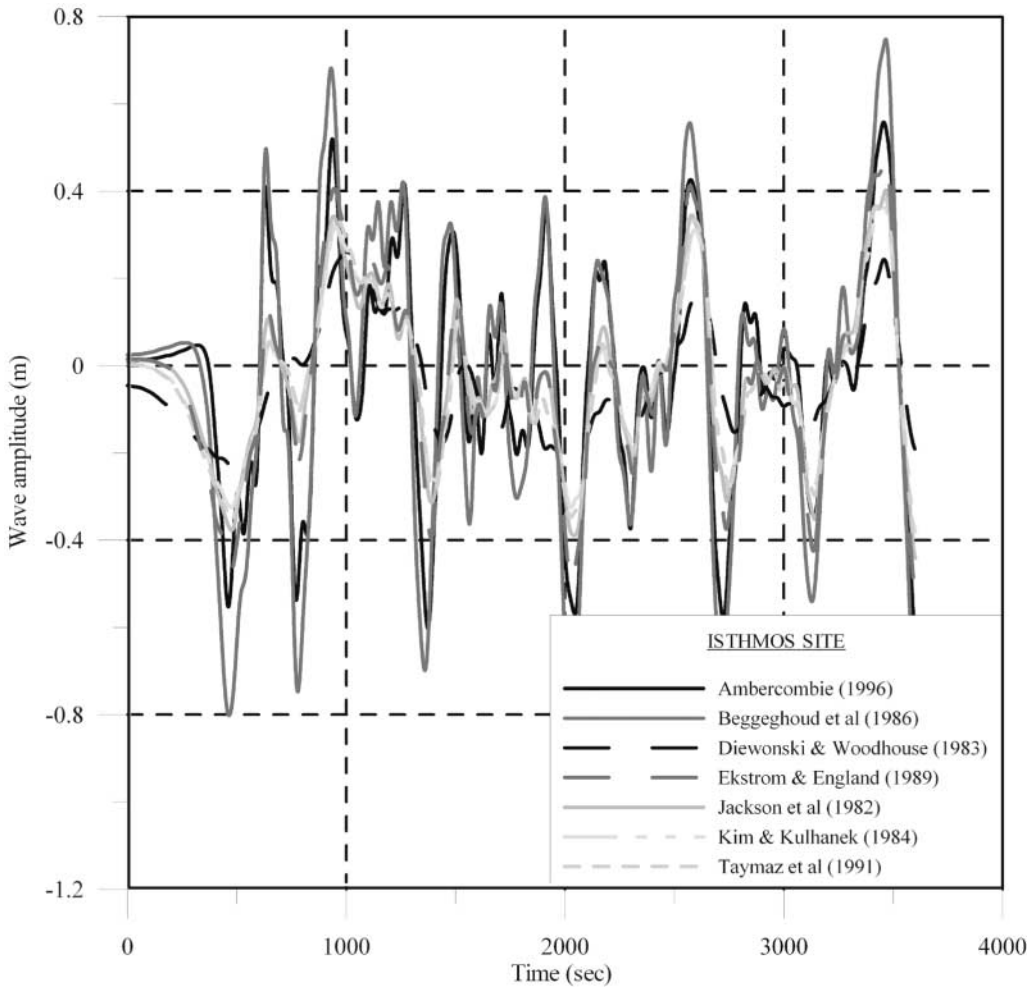

Figure 4. Calculated mareograms at Isthmos site, for each one of the source mechanisms of Table 1 and at an isobath of 8 m.

ulations. As the wave propagates into shallower waters h_{max} decreases and by decreasing Δx we can maintain a constant Δt (Goto and Ogawa, 1982).

The numerical model employed in this study was developed by Tohoku University (Goto *et al.*, 1997), namely the Numerical Analysis Model for Investigation of Near-field Tsunamis version 2 (TUNAMI-N2). Although the model is a nonlinear shallow-water wave tsunami-propagation model, it uses linear theory for the deep-water region and shallow-water theory in the near-shore region.

The algorithm solves the governing equations by the finite-difference technique with leap-frog scheme. The bathymetry of the Corinth Gulf was digitized from nautical maps with a grid size of 80 m. The timestep is selected as 6 sec to satisfy the stability condition described in equation (8).

Following this procedure we calculate the corresponding mareograms for each one of the rupture models depicted in Table 2 at the coastal location of the town of Isthmos and at the depth of 8 m (Fig. 4) The only available tide gauge record at that location shows a maximum water height of about 40 cm. Judging from these results we can see that there is a 50% variation in the expected tsunami amplitudes among various models. The model of Ekstrom and England (1989) results in tsunami amplitude close to the recorded one and is selected for further numerical modeling as an example only of a uniform slip model.

Next, the corresponding mareograms expected at the coastal locations of the towns of Isthmos, Loutraki, Galaxidi, and Xilocastro are calculated and depicted in Figure 5. Judging from this figure, we can see that for this particular slip model, the tsunami arrives first at the city of Xilocastro, next (after 4 min) almost simultaneously at the cities of Loutraki and Isthmos, and finally at the city of Galaxidi.

To get a clear view of the way the tsunami propagates all over the Corinth Gulf, snapshots of surface displacement at given time intervals of 1 min are calculated and presented in Figure 6, and Figure 7 presents the expected maximum water levels.

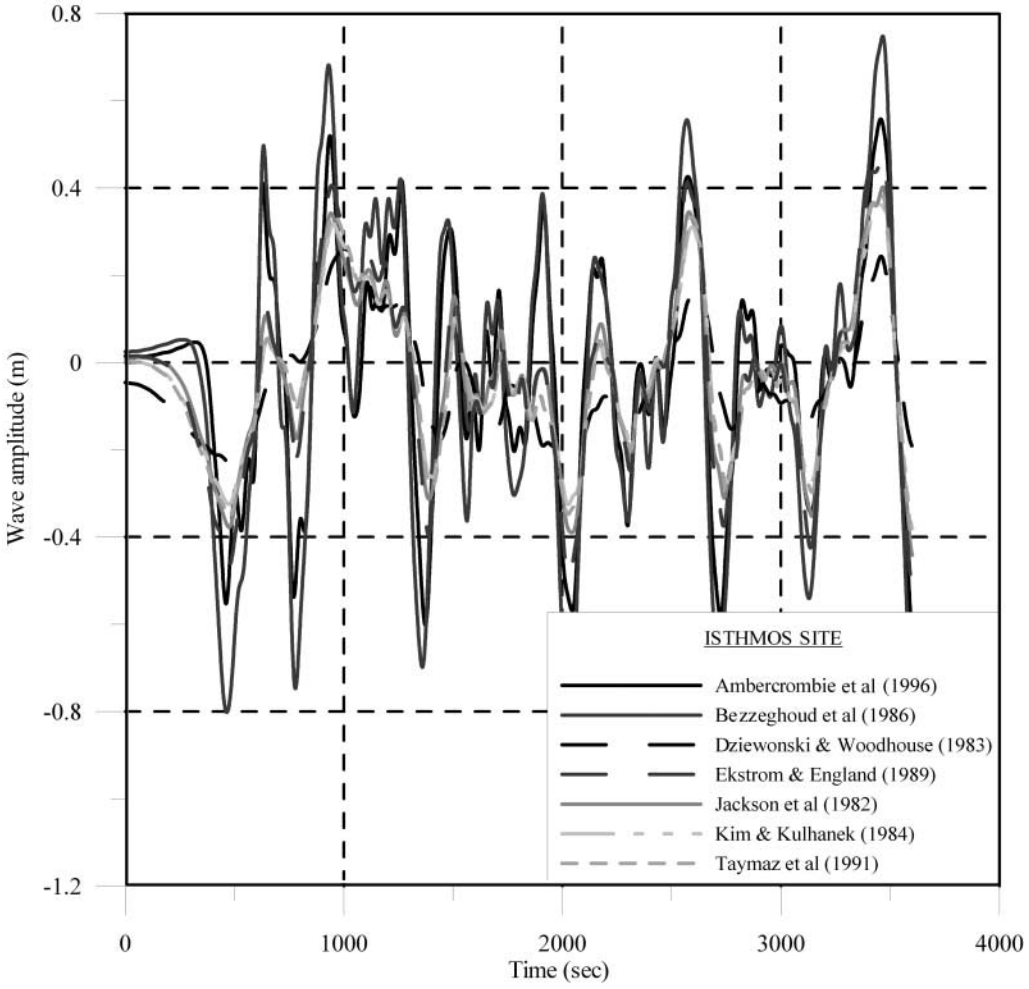

Figure 5. Expected mareograms at the coastal regions of Isthmos, Loutraki, Xilokastro, and Galaxidi (at an isobath of 8 m) for the Ekstrom and England (1989) source mechanism.

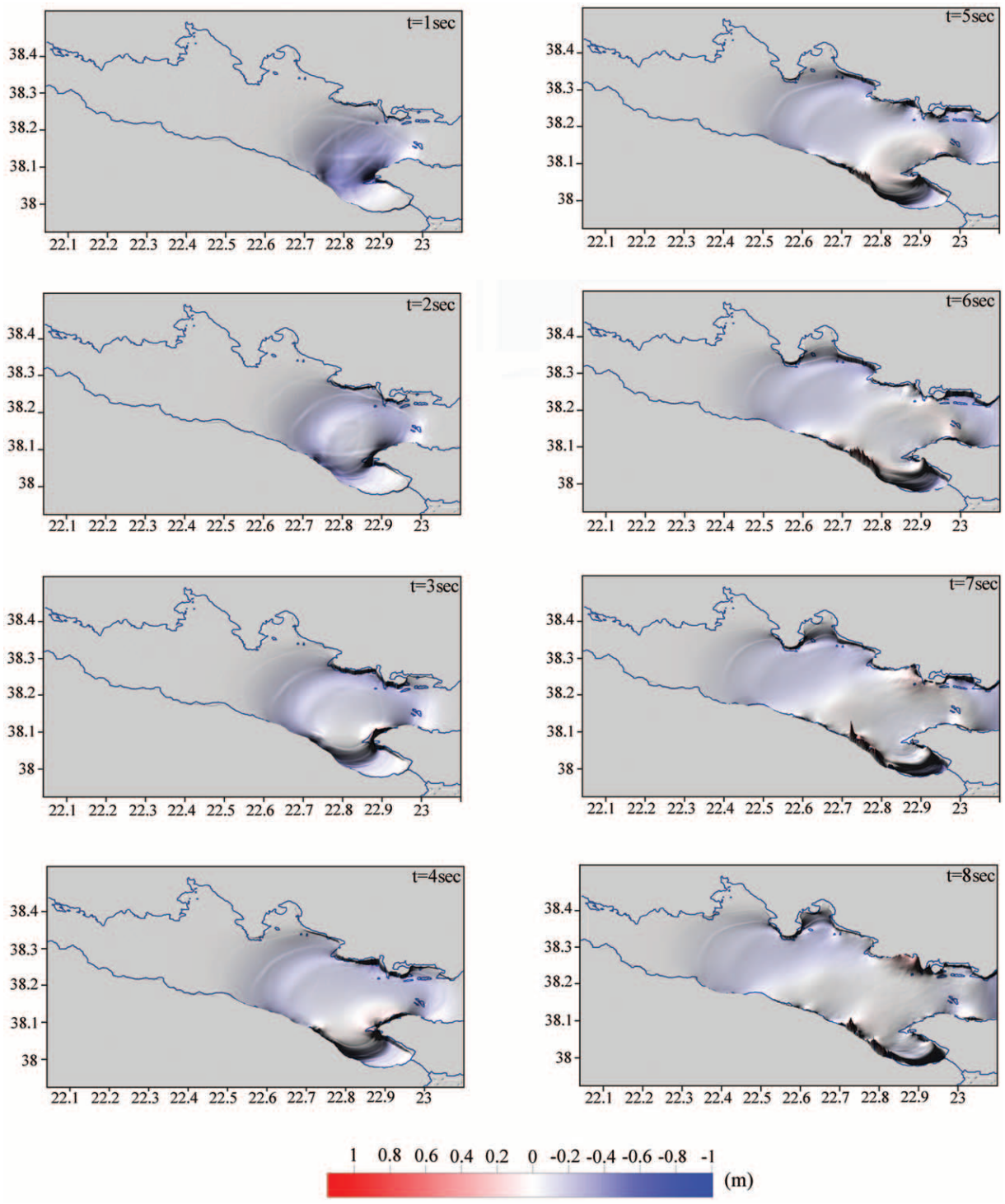

Figure 6. Snapshots of tsunami propagation for the Ekstrom and England (1989) model at 1-min time intervals.

Effect of Rupture Complexity

Whereas the characterization of earthquake rupture using a uniform slip dislocation or several dislocations that span the width of the rupture zone is common in tsunami modeling (i.e., Imamura *et al.*, 1995; Piatanesi *et al.*, 1996; Satake and Tanioka, 1999) recent research (i.e., Geist and Dmowska, 1999; Geist, 2002; Legg *et al.*, 2004) demonstrates that complex rupture processes have important effects on tsunami generation and near-shore amplitudes. Real earthquakes have nonuniform slip distributions, often involving multiple fault segments and high-slip patches.

As discussed by Freund and Barnett (1976) and Rudnicki and Wu (1995), the assumption of uniform slip implies

that deformation is concentrated at the edges of rupture. On the other hand, variable slip in the dip direction for a dip-slip fault, such as the Perachora fault, will result in concentrated deformation near the center of the rupture zone and, hence, substantially higher vertical displacements and therefore higher initial tsunami amplitudes (Geist and Dmowska, 1999).

The most accurate representation of the local tsunami wave field is therefore derived from complete knowledge of slip distribution during the rupture process. Seismic inversion simple models provide an initial assessment of real earthquake variability with regard to the wavelengths and scales involved in local tsunami generation. On the other hand we cannot accept that the details of the fault rupture tend to be smoothed out at the seafloor vertical displacement and initial tsunami wave height in the elastic dislocation model, a fact that might hold for deep subduction earthquakes but not for near-field shallow-fault tsunami modeling as in the Perachora fault.

By holding source geometry and average slip constant (hence, constant seismic moment), the stochastic source model produces a wide range of slip-distribution patterns that are consistent with the high-frequency fall-off observed in the far-field seismic displacement spectrum denoted by $\omega^{-\gamma}$ and with the *b*-value in aftershock sequences. The corresponding slip distribution follows a fractal scaling relationship in which the fractal exponent is linked to γ (Tsai, 1997).

Since we have no information on the characteristic spectral decay for eastern Corinth Gulf events, a radial wavenumber slip spectrum that falls off as k^{-2} is used (Herrero and Bernard, 1994), which corresponds to the generic ω^2 model of Aki (1967). The phase of the slip spectrum is randomized to produce slip-distribution patterns characterized by a single region of moment release or multiple subevents (Geist, 2005).

By holding source geometry and average slip constant, that is, keeping a constant seismic moment, the stochastic source model is used to examine the effect that different slip-distribution patterns have on local tsunamis in the region of the eastern Corinth Gulf. A flow chart depicting the methodology followed in this study is presented in Figure 8.

The 2D slip distribution $D(k)$, where $k = (k_x, k_z)$, for a rectangular fault of length L and width W can be described (Herrero and Bernard, 1994; Gallovic, 2002) by its spatial Fourier spectrum:

$$D(k_x, k_y) = \frac{\Delta\bar{u}LW}{\sqrt{1 + \left[\left(\frac{k_x L}{K}\right)^2 + \left(\frac{k_z W}{K}\right)^2\right]^2}} e^{i\Phi(k_x, k_z)}, \quad (9)$$

where Δu denotes the mean slip and K is an optional parameter allowing consideration of generalized corner wavenumbers K/L and K/W. The phase spectrum Φ is considered random at any wavenumber, except for circle $k^2 \leq (1/L)^2 + (1/W)^2$ for which the phase is chosen in such a way as to obtain the final slip concentrated in the center of the fault.

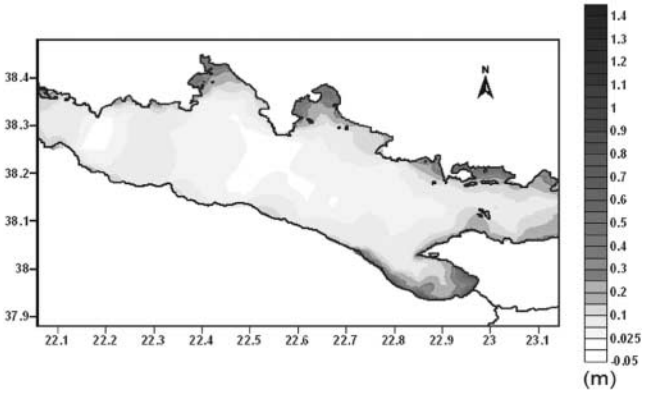

Figure 7. Maximum water level calculated all over the coastal zone of Corinth Gulf and at an isobath of 8 m.

The slip distribution is generated in the following way (Gallovic, 2002). Random numbers are distributed in spatial domain on the discretized fault. This function (2D discrete random signal) is transformed to the wavenumber Fourier spectrum. The amplitudes of the spectrum are substituted by the amplitude term in equation (9).

The phases inside the circle $k^2 \leq (1/L)^2 + (1/W)^2$ are changed to get the center of the whole dislocation in the center of the fault ($\Phi(k_x, k_z) = -2\pi(k_x L/2 + k_z W/2)$). The other phases (which are still random) remain. The spectrum is then transformed back to the spatial domain. This procedure can return negative values of the slip in certain locations of the fault. Such undesirable negative values are replaced by zeros. Finally, the slip is tapered on the edges of the fault by a double-cosine spatial window and the distribution is normalized to conserve the given seismic moment. The K parameter characterizes the slip roughness. The larger or smaller K is, the more or less dramatic slip variation over the fault is obtained.

Many investigators (e.g., Pelinovsky and Mazova, 1992; Tadepalli and Synolakis, 1996) have shown that parameters such as leading wave steepness, polarity, and amplitude ratio of the leading phases all have a significant effect on tsunami run-up. The most accurate representation of the local tsunami wave field is therefore derived from complete knowledge of how slip is distributed throughout the area of rupture (Geist, 2002).

The variability in tsunami amplitude in the region is computed using rupture geometry identical with that of the 1981 m_b 6.7 earthquake (e.g., Hubert *et al.*, 1996). Different slip distributions are calculated using the stochastic source model (Herrero and Bernard, 1994). We take as total seismic moment for these events the mean seismic moment reported by various investigators (depicted in Table 1), which is estimated as M_0 8.8 $\times$ 10^{18} N m.

The coseismic vertical displacement field is calculated

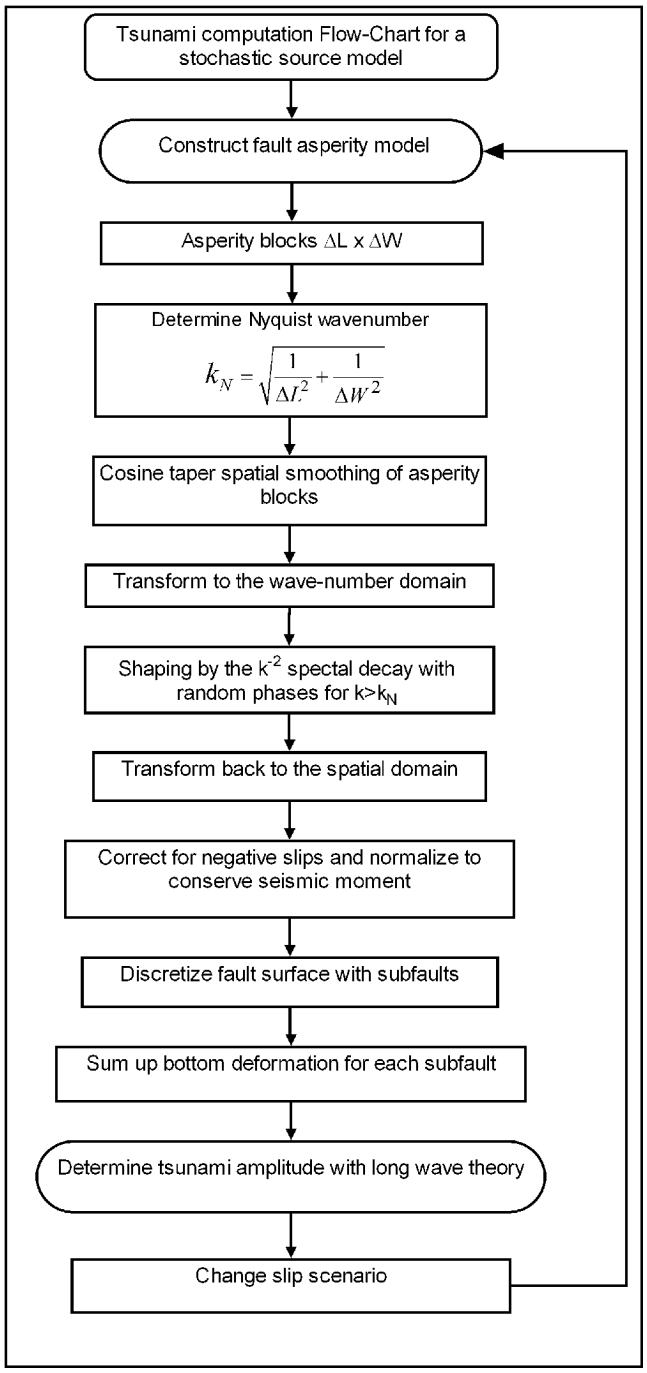

Figure 8. Flow chart depicting the basic steps of the stochastic slip tsunami modeling procedure followed in the present investigation.

for each stochastic slip distribution by summing up the elastic dislocation expressions of Okada (1985) for each fault element. A small grid size (Fig. 9) is used in calculating both the slip distribution ($\Delta s = 1$ km) and seafloor displacement ($\Delta x = 0.5$ km). Fault surface element dimension (Δs) less than or equal to the source depth can adequately represent the seafloor-displacement field (Geist and Dmowska, 1999 Geist, 2002).

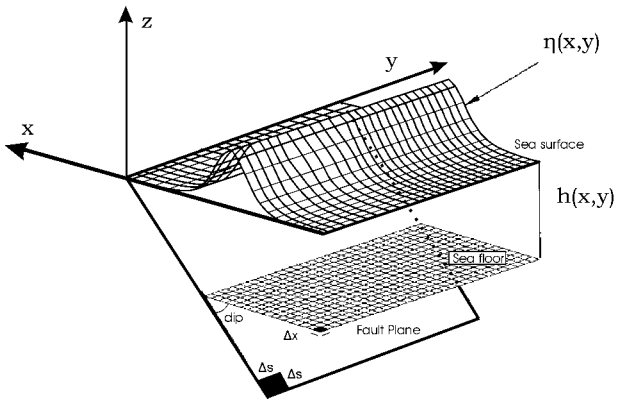

Figure 9. Sketch of coordinates and some flow property definitions of the Perachora fault. Coseismic vertical displacement of the seafloor is calculated from variable slip within a fault plane discretized at Δs. A grid size of Δx is used for the finite-difference simulation of the tsunami propagation.

Calculations of seafloor displacements are made assuming a homogeneous elastic structure (Poissons solid). The effect of elastic inhomogeneity on surface displacements and tsunami waveforms is not included in this study. The near-shore tsunami amplitude values predicted in this study ignore the possibility of large submarine landslides being triggered by the earthquake, and this study focuses on the tectonic sources only. A large earthquake on the Perachora fault system could possibly generate a large landslide that affects the steep submarine slopes and generate tsunami wave energy additional to that of the tectonic displacement.

Figure 10 presents the synthetic mareograms calculated at Loutraki site for two different slip distributions. The effect of the shallow asperity model on the tsunami amplitude is obvious. On the same figure, we also depict the histograms of peak near-shore tsunami amplitude (PNTA) for 50 different slip distributions at the cities of Galaxidi (GAL), Xilokastro (XIL), and Loutraki (LOU) and at an isobath of 8 m. From this example we can see that self-affined irregularities of the slip distribution result in significant variation on the local tsunami wave field and that a broad range of synthetic slip-distribution patterns have to be generated by the stochastic source model to reveal the variability of local tsunami amplitudes in a particular region.

Judging from the preceding we can say that the problem of forecasting tsunami hazards in a region is mainly in determining the range of tsunamis that can be produced by different combinations of source parameters. Even if all of the geometric parameters of a "scenario earthquake" are prescribed, there would be a large uncertainty in determining the ensuing tsunami because of the difficulty in formulating a "characteristic" slip distribution (Geist, 1999). Although seemingly random, earthquake slip distributions can be thought of in terms of stochastic models. Such models can be developed to construct an infinite number of different slip

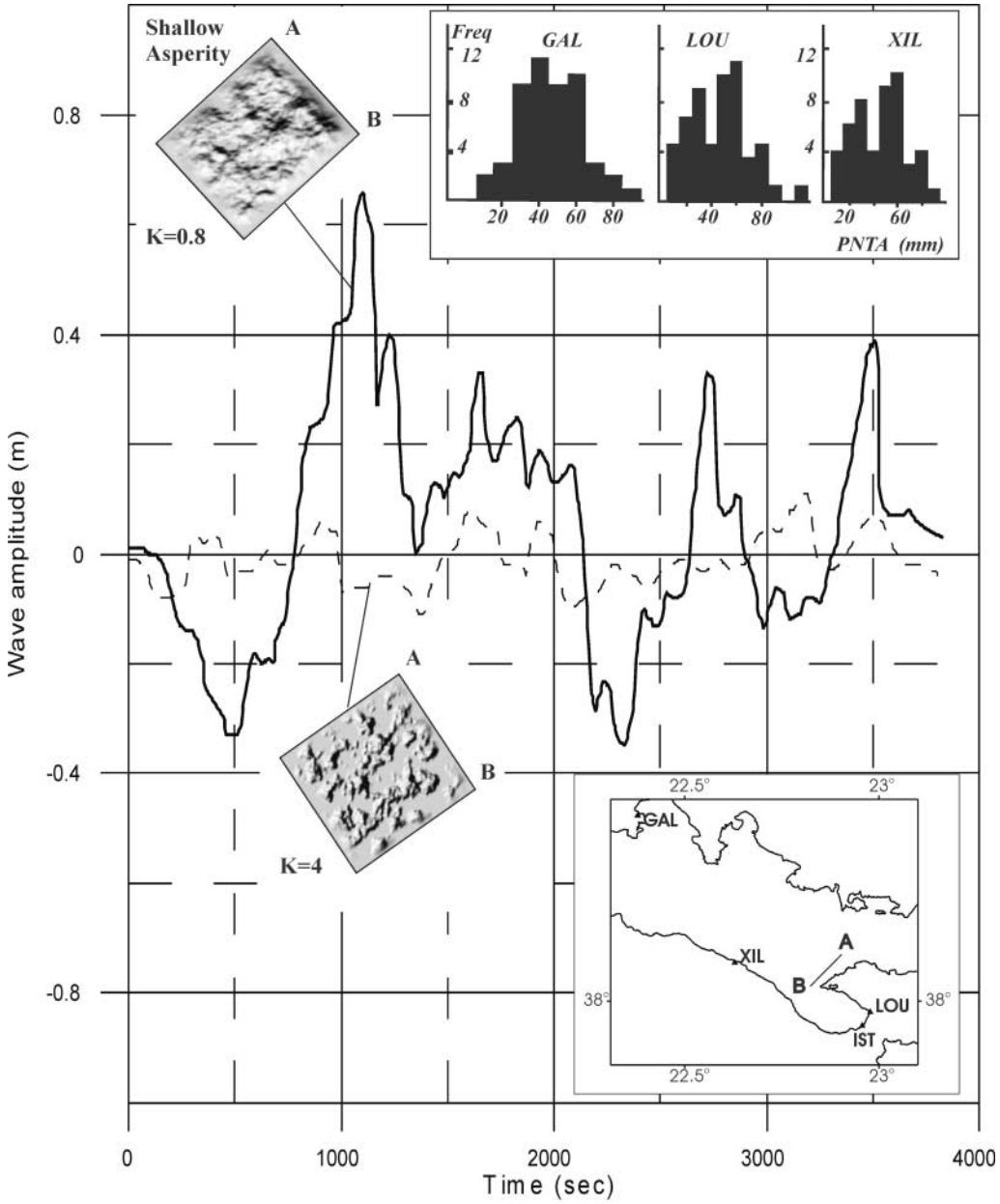

Figure 10. Calculated mareograms at Loutraki (LOU) site for two different slip distributions with $K = 0.8$ (shallow asperity) and $K = 4$ (distributed slip) but with identical fault-plane geometry and seismic moment. Patch of shallow slip results in considerably higher tsunami amplitudes. Histograms of Peak Near shore Tsunami Amplitudes (PNTA) for 50 slip scenarios are also depicted at an isobath of 8 m, for the cities of Loutraki, Galaxidi (GAL), and Xilokastro (XIL).

scenarios that can be used to gauge the range of possible tsunamis from an earthquake of a particular magnitude and location by employing Monte Carlo-type simulations.

Conclusions

The purpose of this investigation was to present the results of numerical simulations of earthquake tsunamis in eastern Corinth Gulf due to the Perachora fault and investigate how they compare with existing observations to be used toward eliminating the tsunami risk of nearby coastal cities.

The results obtained could be used to understand the tsunami risk for the shores of eastern Corinth Gulf where the coastline is densely populated and widely used for many purposes, especially during the summer season.

Furthermore, results from this investigation stress the importance of rupture complexity on the local tsunami wave

field. Hence, by adopting the stochastic source model one can generate a broad range of synthetic slip distributions and examine the variation of expected local tsunami amplitudes due to a specific fault.

This study indicates the importance of constructing local tsunami hazard assessments using probabilistic techniques rather than from a simplified elastic dislocation representation of the earthquake source.

Acknowledgments

We thank Philippe Watts and Eric Geist for insightful information concerning the tsunami simulation and stochastic slip generation algorithms, respectively. Frantisek Gallovic kindly provided the numerical code for the stochastic source modeling. We are obliged to Prof. David Pollard (Stanford University) for providing the Poly 3D Software. We also thank two anonymous reviewers for their useful comments. This work was supported, in part, by EC Grants IST-2000-26450-AEGIS and STREP-2005-04043-3HAZ

References

Abercrombie, R. E., I. G. Main, A. Douglas, and P. W. Burton (1995). The nucleation and rupture process of the 1981 Gulf of Corinth earthquakes from deconvolved broadband data, *Geophys. J. Int.* **120,** 393–405.

Aki, K. (1967). Scaling law of seismic spectrum, *J. Geophys. Res.* **72,** 1217–1231.

Bezzeghoud, M., A. Deschamps, and R. Madariaga (1986). Broadband modelling of the Corinth, Greece earthquake of Febrtary and March 1981, *Ann. Geophys.* **4,** 301–314.

Brocchini, M., R. Bernetti, A. Mancinelli, and G. Albertini (2001). An efficient solver for nearshore flows based on the WAF method. *Coastal Eng.* **43,** 105–129.

Brooks, M., and G. Ferentinos (1984). Tectonics and sedimentation in the Gulf of Corinth and the Zakynthos and Kefallinia channels, western Greece, *Tectonophysics* **101,** 25–54.

Dean, R. G., and R. A. Dalrymple (1984). *Water Wave Mechanics for Engineers and Scientists*, World Scientific Publishing Co., Singapore, 353 pp.

Doutsos, T., and G. Poulimenos (1992). Geometry and kinematics of active faults and their seismotectonic significance in the western Corinth-Patra rift (Greece), *J. Struct. Geol.* **14,** 689–699.

Dziewonski, A. M., and J. H. Woodhouse (1983). An experiment in systematic study of global seismicity: centroid moment tensor for 201 moderate and large earthquakes of 1981, *J. Geophys. Res.* **88,** 3247–3271.

Ekstrom, G., and P. England (1989). Seismic strain rates in regions of distributed continental deformation, *J. Geophys. Res.* **94,** 10,231–10,257.

Freund, L. B., and D. M. Barnett (1976). A two dimensional analysis of surface deformation due to dip-slip faulting, *Bull. Seism. Soc. Am.* **66,** 667–675.

Fujima, K. (2001). Long wave propagation on large roughness, ITS Proceedings, Session 7, no. 7-22, 891–895.

Fujima, K., K. Masamura, and C. Goto (2002). Theoretical examinations of long-wave damping by sea bottom friction, *Coastal Eng. J.* **44,** no. 3, 217–245.

Gallovic, F. (2002). High frequency strong motion synthesis for k^{-2} rupture models, *MSc. Thesis*, Charles University, Prague Faculty of Mathematics and Physics, 80 pp.

Geist, E. L. (1999). A stochastic source model for estimating local tsunami hazards, *Seism. Res. Lett.* **70,** 221–225.

Geist, E. L. (2002). Complex earthquake rupture and local tsunamis, *J. Geophys. Res.* **107,** ESE 2-2–2-16.

Geist, E. L. (2005). Local tsunami hazards in the Pacific NW from Cascadia subduction zone earthquakes, in *Earthquake Hazards of the Pacific NW Coastal and Marine Regions*, R. Kayen (Editor), *U.S. Geol. Surv. Profess. Pap. 1661-B.*

Geist, E. L., and R. Dmowska (1999). Local tsunamis and distributed slip at the source, *Pure Appl. Geophys.* **154,** 485–512.

Goto, C., and Y. Ogawa (1992). Numerical method of tsunami simulation with the leap-frog scheme. Department of Civil Engineering, Tohoku University. Translated for the TIME project by N. Shuto.

Goto, C., Y. Ogawa, N. Shuto, and N. Imamura (1997). Numerical method of tsunami simulation with the leap-frog scheme (IUGG/IOC Time Project), IOC Manual, United Nations Educational Scientific and Cultural Organization (UNESCO), no. 35.

Hatzfeld, D., V. Karakostas, M. Ziazia, I. Kassaras, E. Papadimitriou, K. Makropoulos, N. Voulgaris, and C. Papaioannou (2000). Microseismicity and faulting geometry in the Gulf of Corinth (Greece), *Geophys. J. Int.* **141,** 438–456.

Herrero, A., and P. Bernard (1994). A kinematic self-similar rupture process for earthquakes, *Bull. Seism. Soc. Am.* **84,** 1216–1228.

Hubert, A., G. King, R. Armijo, B. Meyer, and D. Papanastasiou (1996). Fault reactivation, stress interaction and rupture propagation of the 1981 Corinth earthquake sequence, *Earth Planet. Sci. Lett.* **142,** 573–585.

Imamura, F., E. Gica, T. Takahashi, and N. Shuto (1995). Numerical simulation of the 1992 Flores Tsunami: interpretation of tsunami phenomena in NE Flores Island and damage at Babi Island, *Pageoph* **144,** no. 3/4, 555–568.

Jackson, J. A., J. Gagnepain, G. Houseman, G. C. P. King, P. Papadimitriou, C. Soufleris, and J. Virieux (1982). Seismicity, normal faulting and the geomorphologicol development of the Gulf of Corinth (Greece): the Corinth earthquakes of February and March 1981, *Earth Planet. Sci. Lett.* **57,** 377–397.

Kim, W. Y., and O. Kulhanek (1984). Source processes of the 1981 Gulf of Corinth earthquake sequence from body-wave analysis, *Bull. Seism. Soc. Am.* **74,** no. 2, 459–477.

Legg, M. R., J. C. Borrero, and C. E. Synolakis (2002). Evaluation of tsunami risk to Southern California cities, National Earthquake Hazards Reduction Programs, ERI Report PF2002-11, 43 pp.

Legg, M. R., M. Eeeri, J. C. Borrero, and C. E. Synolakis (2004). Tsunami hazards associated with the Catalina fault in Southern California, *Earthquake Spectra* **20,** no. 3, 917–950.

Moretti, I., D. Sakellariou, V. Lykousis, and L. Micarelli (2003). The gulf of Corinth: an active half graben? *J. Geodyn.* **36,** 323–340.

Okada, Y. (1985). Surface deformation due to shear and tensile faults in a half space, *Bull. Seism. Soc. Am.* **75,** 1135–1154.

Okal, E. A. (1982). Mode-wave equivalence and other asymptotic problems in tsunami theory, *Phys. Earth. Planet. Interiors.* **30,** 1–11.

Papadopoulos, G. A. (2003). Tsunami hazard in the Eastern Mediterranean: strong earthquakes and tsunamis in the Corinth Gulf, Central Greece, *Nat. Hazards* **29,** 437–464.

Pelinovsky, E. N., and R. K. Mazova (1992). Exact analytical solutions of nonlinear problems of tsunami wave run-up on slopes with different profiles, *Nat. Hazards* **6,** 227–249.

Peregrine, D. H. (1967). Long waves on a beach, *J. Fluid Mech.* **27,** 815–827.

Piatanesi, A., S. Tinti, and I. Gavagni (1996). The slip distribution of the 1992 Nicaragua earthquake from tsunami runup data, *Geophys. Res. Lett.* **23,** 37–40.

Plafker, G., and J. P. Galloway (1989). Lessons Learned from the Loma Prieta, California, Earthquake of October 17, 1989, *U.S. Geol. Surv. Circular 1045*, 48 pp.

Ramming, H. G., and Z. Kowalik (1980). Numerical modeling of marine hydrodynamics, Elsevier, New York, 368 pp.

Roberts, S., and J. Jackson (1991). Active normal faulting in central Greece: an overview. in *The Geometry of Normal Faults*, A. M. Roberts, G. Yielding, and B. Freeman (Editors), Geol. Soc. of London, Special Publication 56, 125–142.

Rudnicki, J. W., and M. Wu (1995). Mechanics of dip-slip faulting in an elastic half-space, *J. Geophys. Res.* **100,** 22,173–22,186.

Sakellariou, D., V. Lykousis, and D. Papanikolaou (1998). Neotectonic structure and evolution of the Gulf of Alkyonides, Central Greece, *Bull. Geol. Soc. Greece* **32,** 241–250.

Satakae, K., and P. G. Somerville (1992). Location and size of the 1927 Lompoc, California, earthquake from tsunami data, *Bull. Seism. Soc. Am.* **82,** 1710–1725.

Satake, K., and K. Tanioka (1999). Sources of tsunami and tsunamigenic earthquakes in subduction zones, *Pageoph* **154,** 467–483.

Shuto, N., T. Suzuki, K. Hasegawa, and K. Inagaki (1986). A study of numerical techniques on the tsunami propagation and run-up, *Sci. Tsunami Hazard* **4,** 111–124.

Stefatos, A., G. Papatheodorou, G. Ferentinos, M. Leeder, and R. Collier (2002). Seismic reflection imaging of active offshore faults in the Gulf of Corinth: their seismotectonic significance, *Basin Res.* **14,** 487–502.

Svendsen, I. A., and U. Putrevu (1994). Nearshore mixing and dispersion, *Proc. R. Soc. London. Ser. A* **445,** 561–576.

Synolakis, C. E., Liu P. L.-F, G. Carrier, and H. H. Yeh (1997). Tsunamigenic seafloor deformations, *Science* **278,** 598–600.

Tadepalli, S., and C. E. Synolakis (1996). Model of the leading waves of tsunamis, *Phys. Rev. Lett.* **77,** 2141–2144.

Taymaz, T., J. A. Jackson, and D. P. McKenzie (1991). Active tectonics of the north and central Aegean Sea, *Geophys. J. Int.* **106,** 433–490.

Thomas, A. M. (1993). Poly 3D: a three-dimensional, polygonal element, displacement discontinuity boundary element computer program with applications to fractures, faults and cavities in the Earth's crust, *M.S. Thesis*, Stanford University.

Tinti, S., and A. Armigliato (2003). The use of scenarios to evaluate tsunami impact in South Italy, *Mar. Geol.* **199,** 221–243.

Titov, V., and F. Gonzalez (1997). Implementation and testing of the method of splitting tsunami (MOST) model, NOAA Technical Memorandum ERL PMEL-112.

Treiman, J. A, K. J. Kendrick, W. A. Bryant, R. K. Rockwell, and S. F. McGill (2002). Primary surface rupture associated with the M_w 7.1 16 October 1999 Hector Mine earthquake, San Bernardino, County, California, *Bull. Seism. Soc. Am.* **92,** 1171–1191.

Tsai, C. P. (1997). Slip, stress drop and ground motion of earthquakes: A view from the perspective of fractional Brownian motion, *Pageoph* **149,** 689–706.

Tselentis, G-A., and K. Makropoulos (1986). Rates of crustal deformation in the Gulf of Corinth (central Greece) as determined from seismicity, *Tectonophysics* **24,** 55–61.

University of Patras
Seismological Lab
Rio 265 00 Greece

Manuscript received 9 June 2005.